I&EC research
Industrial & Engineering Chemistry Research

pubs.acs.org/IECR
Article

Stability Valorization of Hydrofluoroolefine HFO-1336mzzE and Its Mixtures under Arc Discharge Conditions

Elisabeth Bilbao, Xinyi Xia, María Luz Alonso, Rosa María Alonso, Jesús Izcara, Josu Izagirre, and José Ignacio Lombraña*

Cite This: *Ind. Eng. Chem. Res.* 2024, 63, 2916–2931

ABSTRACT: Sulfur hexafluoride (SF_6) has been conventionally used as an insulating gas in switchgear. However, owing to its high Global-warming Potential (GWP), the United Nations Framework Convention on Climate Change (UNFCCC) calls for its replacement with alternative gases. In this work, hydrofluoroolefine HFO-1336mzzE is analyzed as an alternative, due to its good dielectric strength and low GWP. For this purpose, the influence of electric discharges on the stability of this gas in mixtures with vector gases (air, CO_2 and N_2) at 20% (v/v) was studied, and the influence of humidity (0, 200, and 500 ppm) and temperature (25 °C, 60 and 120 °C) was determined. Electric arc discharge was conducted by a gas-insulated medium voltage switchgear prototype specifically designed for this work. Its main characteristic is the uniform distribution of the dissipated energy, facilitating better reproducibility of the results. The degradation of HFO-1336mzzE was monitored by gas chromatography coupled to mass spectrometry (GC/MS) sampling in addition to online measurement using Near-infrared spectroscopy (NIR). The degradation rate (DR) was measured by assessing the concentrations of the different degradation gases occurring in each experiment. The results were evaluated by using density functional theory (DFT) and transition state theory (TS). Finally, the DR analysis was completed with a study of coke formation for prolonged discharge periods. The gas mixture containing CO_2 showed a higher stability compared to those containing air or N_2, with temperature being the most decisive factor. A declining trend in the degradation rate tending toward stabilization was observed, rendering CO_2 the preferred carrier gas.

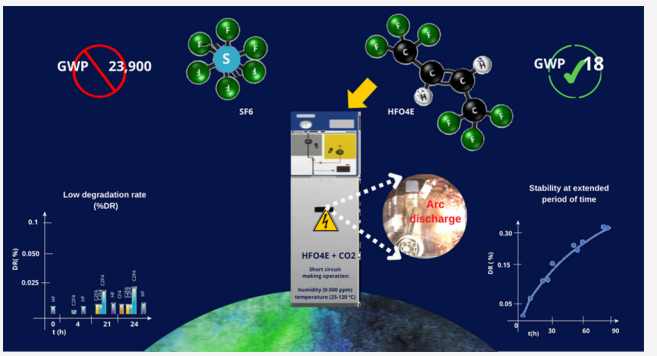

1. INTRODUCTION

The European Union (EU) is committed to drastically reducing greenhouse gas (GHG) emissions in its Member States by 2050, going as far as proposing to achieve a climate-neutral economy. This European commitment to decarbonize the economy increases the demand for electricity, boosting the electricity generation and distribution market. As a result, the sector has been subjected to increasingly strict sustainability and energy efficiency regulations over the years. Moreover, the electricity sector is affected by dynamic effects that must be considered in the decision-making processes. Dynamic effects include those arising from climate change, the evolution of the renewable component of the electrical mix, and the criticality of materials used in the manufacture of equipment.

Notably, the environmental impact of the technologies used to manufacture the equipment makes it necessary to research new insulation materials for medium-voltage switchgear to continue to guarantee the safety,[1] continuity, and reliability in the supply of electrical energy. To date, gas-insulated switchgear (GIS) made of sulfur hexafluoride (SF_6) has been the most widely used insulation material worldwide.[2] SF_6 is a nontoxic, colorless, odorless, nonflammable gas with exceptionally good insulation and arc interruption properties. Its insulating capacity is 2.5 times higher than air, whereas its arc extinguishing is 100 times higher than the air.[3] However, the Global-warming potential (GWP) of SF_6 is 23,900 CO_2 eq,[4,5] and its extremely stable structure allows it to remain in the atmosphere for 3,200 years without reacting with atmospheric water vapor.[6] Importantly, emissions of fluorinated gases account for 2.1% of total greenhouse gas emissions.[7]

Taking these data and the United Nations Framework Convention on Climate Change (UNFCCC), which set a goal of limiting and reducing greenhouse gas emissions in the Kyoto Protocol[8,9] (2005), signed by 192 countries, into consideration, the replacement of SF_6 with alternative gases with equivalent properties and no environmental impact emerges as a significant issue for electrical and electronic companies.

Received: November 2, 2023
Revised: January 9, 2024
Accepted: January 12, 2024
Published: February 12, 2024

https://doi.org/10.1021/acs.iecr.3c03835
Ind. Eng. Chem. Res. 2024, 63, 2916–2931

Table 1. Dielectric Gases as Alternatives to SF_6 and Their Comparison in Terms of Their Physical Properties

Gas	Dielectric strength relative to SF_6	Lifetime (years)	GWP (100 years)	CAS number
SF_6	1[15,16]	3,200[15−17]	23,900[15,16]	2551-62-4
N_2	0.36[16]	0[16]	0[16]	7727-37-9
CO_2	0.30[16]	∞[16]	1[16]	124-38-9
Air	0.30[16]	∞[16]	≈0[16]	132259-10-0
C_2F_6	0.78−0.79[16]	10,000[15]	9,200[16]	76-16-4
C_3F_8	0.96−0.97[16]	2,600[16]	7,000[16]	76-19-7
c-C_4F_8	1.25−1.31[16]	3,200[16]	8,700[16]	115-25-3
C_4F_7N	2.74[16]	35[16]	2,700[16]	375-00-8
$C_5F_{10}O$	2[15]	0.04[15]	<1[15]	375-62-2
$C_6F_{12}O$	2.5[15]	0.0019[15]	<1[15]	40573-09-9
HFO 1336mzzE	1.5[17]	0.06[17]	18[17]	66711-86-2

Furthermore, under the Montreal Protocol (2016), chlorofluorocarbons (CFCs) and hydrochlorofluorocarbons (HCFCs) were replaced by hydrofluorocarbons (HFCs) and perfluorocarbons (PFCs).[10] However, some of these gases, such as C_2F_6, C_3F_8, c-C_4F_8, and C_4F_7N, have a high GWP and, in the worst-case scenario, can reach 9,200 CO_2 eq in 100 years, as well as an atmospheric lifetime of 10,000 years.[11] More eco-friendly alternatives to SF_6 in gas insulated equipment (GIE) have been explored in recent years, such as ketones, fluorinated nitrile, and hydrofluoro-olefins. In these studies, different qualities of the gases have been analyzed and compared, such as dielectric properties, arc-quenching, stability decomposition, material compatibility, and biosafety.[12] Ormazabal Corporate Technology (Spain, Bizkaia) suggested hydrofluorolefine 1,1,1,1,4,4,4-hexafluorobut-2-ene or HFO-1336mzz (E), hereafter referred to as HFO4E, as a viable alternative to SF_6 due to its good dielectric strength and low GWP. Moreover, five EU countries have recently submitted a proposal to the European Chemicals Agency (ECHA) to restrict the use of compounds containing $-CF_3$ or $-CF_2-$ in their chemical structure (fluorinated compounds in general).[13] However, despite this pressure, the use of fluorinated gases, such as those studied here, should be positively valued considering their life cycle advantages (carbon footprint) are considerably more favorable than nonfluorinated gas alternatives.

Table 1 shows the properties of the gas chosen in this work, HFO4E, in comparison with those of SF_6, the previously mentioned perfluorocarbons, and the compounds chosen to complement the mixture with HFO4E: CO_2, N_2, and air. The main advantage of these natural gases is their null or lower GWP compared to that of synthetic gases. The GWP is one for CO_2 and zero for N_2 and dry air. It is worth noting that the dielectric strength of CO_2 mixtures is higher than that of N_2 and has a certain capacity to recover its dielectric strength.[14]

HFO4E, shown in Figure 1, is a colorless, nonflammable, nonexplosive, nontoxic, highly thermally stable gas commonly used as a refrigerant.[18] However, data on the use of HFO4E as a dielectric insulator in electrical and electronic applications are scarce. Notably, its dielectric strength is 1.5 times higher[17] than that of SF_6, and it has an exceptionally low GWP compared to SF_6 with a GWP 100-year value of 18 CO_2 equivalent.[17] Moreover, the compound remains in the atmosphere for only 22 days. However, its boiling point is only 7.5 °C. Hence, it must be mixed with a vector gas to avoid condensation at low temperatures.

Furthermore, more information on the decomposition of HFO4E is required.[19,20] Therefore, it is important to conduct studies on the behavior of this gas under different operating conditions such as GIS, humidity, temperature, and electric arc. In addition, the decomposition rate of HFO4E, the generated byproducts, and its dielectric properties may impact the lifetime of the equipment. The stability of HFO4E was studied with the following vector gases: air, CO_2, and N_2. The main characteristics of each gas and the reason for their choice are given below.

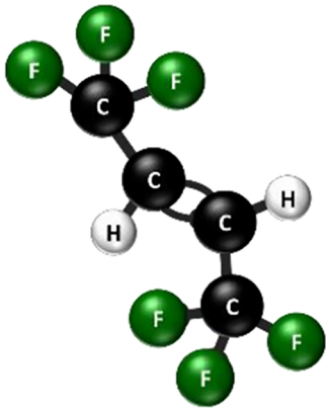

Figure 1. Molecular structure of HFO4E.

Dry air has no GWP and exhibits a dielectric strength of approximately 1/3 of that of SF_6 gas. Therefore, some studies[21] suggest that the pressure inside the switchgear must be tripled, whereas, in some cases, the current intensity must be reduced to achieve the same performance as the SF_6. To address this issue, dry air is mixed as a vector gas with other gases of higher dielectric strength to reduce the consumption of this gas and to decrease the boiling temperature.

N_2, like air, has a dielectric strength that is lower than SF_6. Hence, as with dry air, it is necessary to increase the pressure inside the switchgear or to increase the size of the equipment to increase the distance between the conductors and between the conductors and the earth to ensure electrical insulation.[22] Mixing with N_2 reduces the consumption of the accompanying gas and solves the problem of liquefaction in areas with low operating temperatures. However, due to the effect of the arc and aging of the equipment,[23] nitrogen can decompose and react with H_2O and/or O_2 to form NO_2.

CO_2, for the same reason as in the previous cases (a low dielectric strength), must be mixed with another gas to replace SF_6 in currently applied equipment without increasing pressure or size.[5]

Recent studies of HFO4E have shown a similar stability to SF_6, presenting itself as an eco-friendly alternative to replace the already limited use of SF_6 in GIE.[24] In some of these studies, the

https://doi.org/10.1021/acs.iecr.3c03835
Ind. Eng. Chem. Res. 2024, 63, 2916−2931

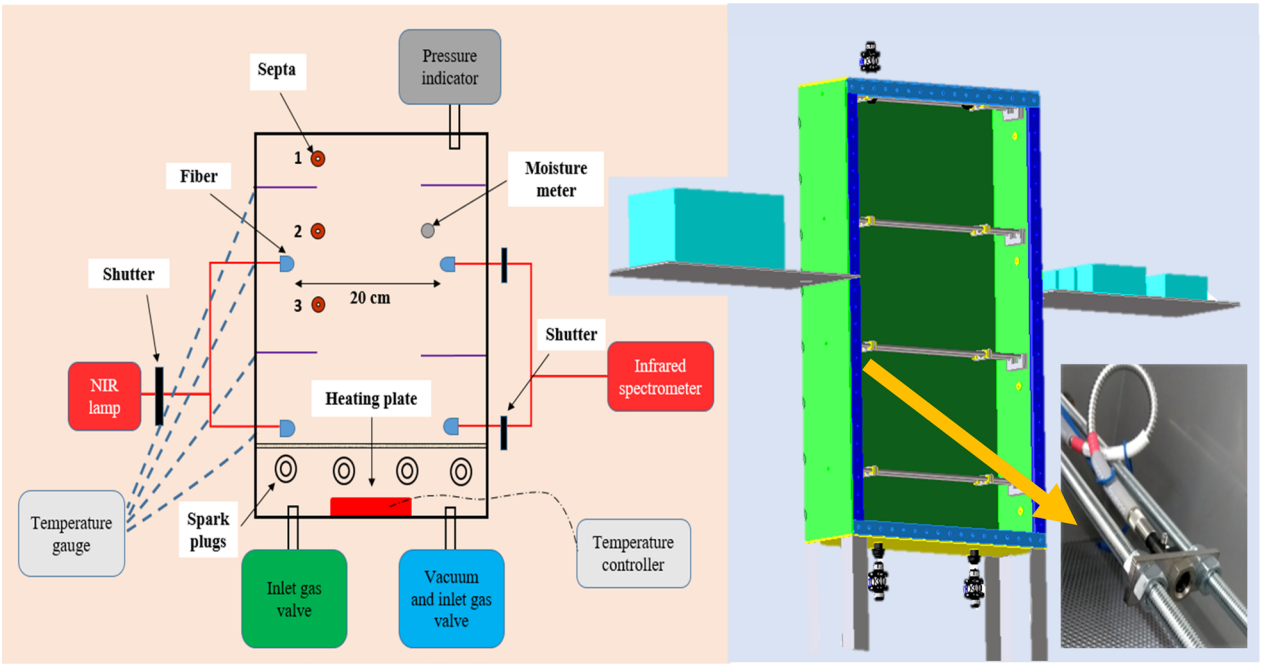

Figure 2. A schematic diagram of the equipment and its 3D representation together with a real image of the NIR fibers.

behavior of HFO4E mixed with CO_2 has also been analyzed, where a positive synergistic effect between both gases has been obtained, in addition to a less sensitive behavior toward electrical field heterogeneity (at HFO4E contents higher than 15%)[25] compared to SF_6. However, while seeking similarity with the insulation performance of SF_6, important aspects such as the stability of the HFO4E mixture under different conditions of use, as discussed in this study, should not be neglected.

The operating conditions of the GIS have been selected based on IEC 62271-1:2017 standards in accordance with previously conducted studies.[20] The temperature limit for the contact and connection was set to 115 °C.

The humidity in the chamber is another crucial factor. The water content in the gas affects its dielectric strength and can lead to corrosion, reducing the life of the equipment. According to IEC 60376 standards, the water content in pure SF_6, as supplied by the manufacturer, must be less than 200 ppmv; however, it usually remains below 50 ppmv.

The electric arc associated with the breaking and making[20] operations of medium-voltage switchgear is one of the key factors in studying the integrity of insulating gases. The arc discharge tests, according to IEC62271-103 standards, were conducted in a sequence of a certain number of discharges, resulting in a corresponding amount of dissipated energy.

Therefore, the primary objective of this research is to investigate the stability of a HFO4E gas misture, when exposed to energy levels equivalent to 100 current setting maneuvers of 630 A and 24 kV. This study was conducted using a mixture of HFO4E gas and a vector gas (N_2, CO_2, or dry air) in an 80:20 (v/v) ratio,[22,23,26,27] to ensure the required insulation performance, at various humidity and temperature conditions.

To achieve this objective, a prototype of GIS was specifically engineered for conducting the experiments. This approach was chosen because conventional arc simulators suffer from the limitation of retaining energy dissipation per unit volume (measured in kilojoules per liter or in units of W per liter, depending on the context) as an equivalence criterion. In cases where researchers aim to accelerate degradation processes,[28] the standard energy dissipation per unit volume may be multiplied by a factor of 10. While this may be suitable for investigating properties like dielectric strength, it is not suitable for studying the physicochemical behavior of gas mixtures. Other authors propose the possibility of studying the evolution of decomposition products in simulation studies based on density functional theory (DFT), transition states (TS), and formation pathways in different environments as well as in the presence of O_2 and humidity[29] or in different processes.[30,31] These simulations provide an overview of the stability of HFO4E. However, important aspects such as the vector gas (N_2, air, or CO_2) and its concentration in the mixture require verification by means of the corresponding series of experiments proposed in this study.

In our study, we used a simulator that ensures a uniform distribution of dissipated energy within a specific ratio of kJ/L·day.

Furthermore, a previously validated method based on gas chromatography coupled to mass spectrometry (GC/MS-TCD) was used to identify and quantify the degradation products.[26,27] In addition, a near-infrared online analyzer (NIRQUEST) (900−1700 nm), which may potentially be implemented in industrial equipment, was used as a qualitative tool to determine the stability of HFO4E. Infrared analysis techniques have previously been used to study other SF_6 replacement gases.[28,32] Here, NIR is proposed to confirm that the amount of HFO4E remains constant, i.e., that there is no significant variation with respect to the total initial concentration value of HFO4E in the mixture. Finally, the results are discussed in light of DFT and TS theories with a double purpose of verifying them while drawing a conclusion on the best conditions for the use of the alternative HFO4E mixture.

2. METHODS

2.1. Assayed Gases. A gaseous mixture of HFO4E (Chemours, Wilmington, USA, with a purity of ≥ 99.95%)

https://doi.org/10.1021/acs.iecr.3c03835
Ind. Eng. Chem. Res. 2024, 63, 2916−2931

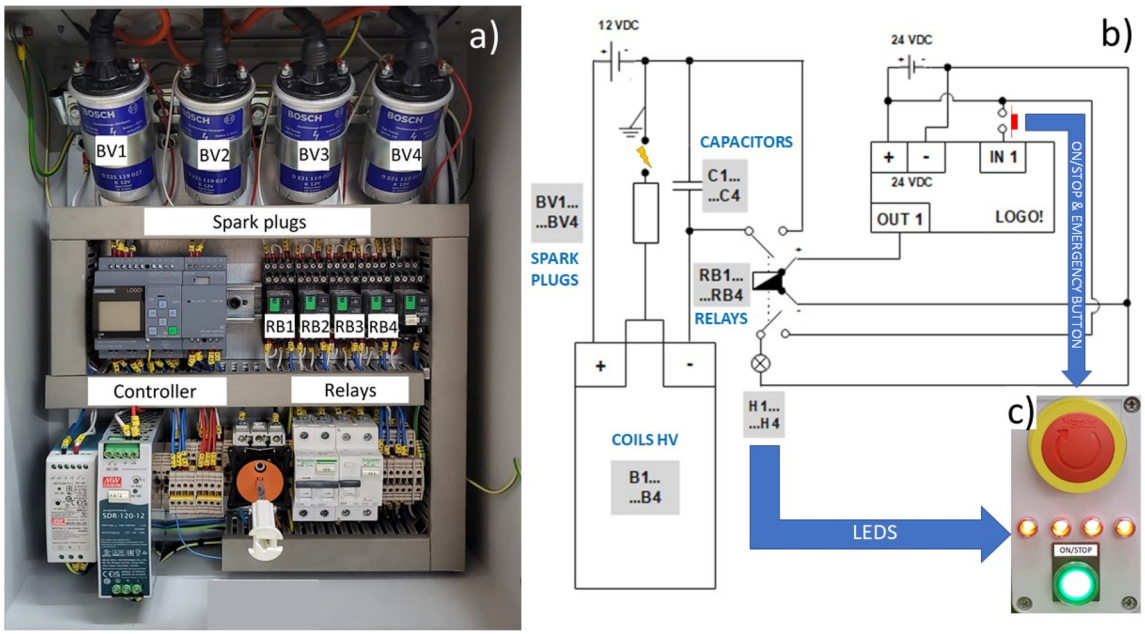

Figure 3. Picture of the arc simulator with the basic elements (a). Electrical diagram of the spark plug operation (b). Spark plug operation indicator with lights and an emergency stop button (c).

and different vector gases, N_2, CO_2, and synthetic air (Air Liquide, Madrid, Spain, with a purity of ≥99.99%) was used for the experiments.

The HFO4E stability experiment was performed under varying conditions: vector gas (air, CO_2 and N_2), humidity (0, 200, and 500 ppm), and temperature (25, 60, and 120 °C). Moreover, this study was conducted in a gas chamber designed to resemble the medium voltage cells used in industry.

2.2. Design and Operation of the GIS Prototype. A 60 L (0.8 m × 0.5 m × 0.15 m) gas chamber was designed and built for this study in collaboration with Aralar SL (Basauri, Bizkaia, Spain) to carry out the experiments. In this chamber, the gases were mixed and concentration measurements were made over time.

The lower position of the cell contains a connection to create a vacuum before introduction of the gas mixture. First, HFO4E was introduced up to 20%, and this concentration was used in all gas mixtures tested to ensure adequate dielectric strength, according to tests carried out at Ormazabal Corp. Tech. regardless of the carrier gas used (air, CO_2 or N_2). Then, the distilled water was added (through the septa 2; see Figure 2) and finally, the vector gas was introduced through the same valve that was used to create the vacuum. The gas chamber was filled to atmospheric pressure and measured with a manometer (WIKA, Klingenberg, Bayern, Germany). The tubes used for the vacuum, the gas supply, and the pressure gauge were made of polytetrafluoroethylene (PTFE).

To generate humidity in the cell, water was injected with a syringe through the second seal of the chamber, as shown in Figure 2. The humidity ranged from 0 (dry gas) to 500 ppm. A data logger (Testo 176 H1, Titisee-Neustadt, Germany) and a humidity/temperature probe (0572 6172, Testo, Germany) were used to continuously monitor the humidity inside the chamber.

A thermal point was created inside the chamber to simulate the operation of the GIS. The operating temperatures were 25 °C, 60 and 120 °C. The temperature gradient was generated by a 100 W hot plate controlled using a PID controller (Red Lion PXU 1/16 DIN, York, PA, USA). The controller was connected to a temperature gauge (Weidmann, Technologies, Dresden, Germany) contained within the hot plate to analyze the difference between the set point and the plate temperature. In addition, a Fotemp 4 temperature meter (OPTOcon AG, Dresden, Germany) provided the temperature profile of the chamber throughout the experiment using four temperature sensors of 0.10, 0.32, 0.52, and 0.68 m height.

An electric arc was simulated by four spark plugs (Bosch no. 0242236633-7A0) located in the lower area. Each was powered by a coil (Bosch 0 221 119 027 Coil pack) with a resistance of 10.5 kΩ. The coils converted the 12 V power supply to 24 kV, creating an electric arc of 1.2 mm in length between the electrodes of the spark plugs in the gas chamber. The electrical discharge may generate an electrical temperature of 60,000 K, dissociating and ionizing the affected gas molecules between the spark plug electrodes. However, due to energy transfer, the plasma temperature in the arc was limited to approximately 6,000 K.[33]

In the present experiment, the simulator operates with the simultaneous action of four spark plugs located in the lower part of the chamber (Figure 3a). The simulator operation scheme is shown in Figure 3b. A controller (Basic 24, SIEMENS, Germany) employs relays RB1−RB4 to regulate the frequency of the drives. These relays produce the desired flashing for the arc discharge on the spark plugs BV1−BV4 and, at the same time, send a signal to the LEDs H1−H4 (Figure 3b and c). The energy dissipated by the arc of each making drive (four spark plugs at once) is 200 mJ.

In the electric arc tests (making), the energy released during the discharges ranged from 0.28 to 0.56 kJ per liter per day and was performed for 16 to 32 discharges per day, each with an energy input of 1.4 kJ. Notably, in the current analysis, the intensity of the electric arc remained consistent and was set at an intermediate value of 0.37 kJ per liter per day.

To maintain this energy level, a frequency of 4667 sparks (0.0002 kJ each) per hour, instead of the actual 1.4 kJ per discharge. Importantly, the estimated volume influenced by the

https://doi.org/10.1021/acs.iecr.3c03835
Ind. Eng. Chem. Res. 2024, 63, 2916−2931

arc simulator was significantly smaller (1.4/0.0002 times) compared to that of a real discharge. As a result, the spark plug simulator achieved a much more uniform distribution of energy in the gas, leading to smaller deviations in the degradation results of HFO4E.

Once the chamber was filled and tempered, the power switch of the system was turned on to generate sparks. One h after the introduction of the gases, the first sample was taken (point 0). For short-term experiments, the remaining samples were measured over 24 h with an arc intensity of 0.37 kJ/L·day. For long-term experiments, the intensity was maintained for 72 h to determine whether the degradation trend remained identical over a longer period.

To analyze the degradation products using GC/MS, gaseous samples were taken from two sealed septa placed at distances of 0.29 and 0.51 m from the bottom (Figure 2) using a Hamilton syringe HDHT (Graubünden, Switzerland). Then, the sample was analyzed at a 1:55 split ratio in the GC/MS equipment using a liner 5183-4647 (Agilent, CA, USA). A Poraplot Q column (25 × 0.25 mm × 8 μm) was used. The temperature of the MS injector was set to 200 °C, whereas the pressure was set to 2.4 psi. The oven temperature was programmed with an initial temperature of 40 °C for 5 min, followed by an increase at a rate of 10 °C·min^{-1} to 75 °C. Finally, the oven temperature was increased at a rate of 5 °C·min^{-1} up to 200 °C.

Analyzing the mass spectra allowed the identification of the decomposition products by chemical interpretation or comparison to the NIST14 mass spectra database. Mass spectra were collected from m/z 15 to 300 (with an electronic impact ionization source of 70 eV).

First, to ensure the repeatability of the ignition and heating systems and the consistency of the humidity percentage in all the conducted experiments, one experiment was selected for each vector gas, and three replicates were carried out at 200 ppm humidity and 60 °C (see experiments marked with r1, r2, and r3 in Table 2).

2.2.1. Fluorine Mass Balance and Degradation Rate. The concentration of nondegraded HFO4E is determined by the fluorine mass balance. The first step is to determine the concentration (in percentage) of the compound formed by degradation using GC-MS analytical data units of abundance, as expressed in eq 1.

$$C_{Pi} = \frac{a_{Pi}}{\sum_{i=P1}^{i=Pn} a_{Pi} + a_{VG} + a_{HF}} \cdot 100 \quad (1)$$

Here, a_{Pi} is the area under the curve of a generic degradation compound P_i, which is divided by the total area of all detected gases: degradation compounds (a_{Pi}), together with that of vector gas (a_{VG}) and HFO4E (a_{HF}), resulting in C_{pi}, which is the concentration percentage of compound P_i.

The concentration of nondegraded HFO4E for time t ($C_{HF,t}$) is obtained by the difference between the initial fluorine content (at time 0) and that in all degradation compounds, as shown in eq 2. Thus, based on the analysis of gas samples, the following equation must be considered:

$$C_{HF,t}W_{HF} = C^*_{HF,0}W_{HF} - \sum_{i=P1}^{i=Pn} C_{P1,t}W_{P1} + \cdots + C_{Pn,t}W_{Pn} \quad (2)$$

Here, C is the concentration HFO4E percentage of each compound, $C^*_{HF,0}$ is the initial concentration (20% v:v) of HFO4E, C_{P1}...C_{Pn} is that of different degradation gases, and W is the mass fraction of fluorine in each fluorinated gas.

The percent concentration of different gases were normalized to C_n, taking as reference the initial concentration of HFO4E, $C^*_{HF,0}$, and $C_{HF,0}$, calculated by the GC-MS software. Thus, eq 3 is used for the degraded gases (P_i).

$$C_{n,Pi} = \frac{C^*_{HF,0}}{C_{HF,0}} \cdot C_{Pi} \cdot f \quad (3)$$

Here, $C_{n,Pi}$ is the normalized concentration (ppmv) of the degradation gas P_i and f is the factor used to convert from percent concentration to ppmv. Similarly, the concentration of normalized HFO4E ($C_{n,HF}$) was obtained from eq 4:

Table 2. Central Composite Experimental Design in Minitab Software for the HFO4E Mixture with Vector Gases

Vector gas	Humidity (ppm)	Temperature (°C)	Experiment name
Air	0	25	A025
	200	25	A225
	500	25	A525
	0	60	A060
	200	60	A260
	200	60	A260r1
	200	60	A260r2
	200	60	A260r3
	500	60	A560
	0	120	A0120
	200	120	A2120
	500	120	A5120
CO_2	0	25	C025
	200	25	C225
	500	25	C525
	0	60	C060
	200	60	C260
	200	60	C260r1
	200	60	C260r2
	200	60	C260r3
	500	60	C560
	0	120	C0120
	200	120	C2120
	500	120	C5120
N_2	0	25	N025
	200	25	N225
	500	25	N525
	0	60	N060
	200	60	N260
	200	60	N260r1
	200	60	N260r2
	200	60	N260r3
	500	60	N560
	0	120	N0120
	200	120	N2120
	500	120	N5120

https://doi.org/10.1021/acs.iecr.3c03835
Ind. Eng. Chem. Res. 2024, 63, 2916−2931

$$C_{n,HF} = \frac{C^*_{HF,0}}{C_{HF,0}} \cdot C_{HF} \cdot f \quad (4)$$

Once the concentration of nondegraded HFO4E, $C_{n,HF}$, has been determined, the degradation rate (DR, %) is determined as the percent of the initial concentration using eq 5:

$$DR = \left(1 - \frac{C_{n,HF}}{fC_{HF,0}}\right) \cdot 100 \quad (5)$$

Similarly, a carbon balance was performed to quantify the amount of degraded HFO4E that is transformed into coke for prolonged periods of exposure to the discharges.

2.2.2. Experimental Design. We employed an experimental design, specifically a central composite design, using the Minitab software to assess how temperature (at 25, 60, and 120 °C) and humidity levels (0, 220, and 500 ppm) affect the stability of HFO4E mixtures. These experiments were conducted under constant arc conditions to determine their impact on the degradation of hydrofluoroolefin within each mixture, where the vector gases used were air, CO_2, and N_2. The response variable analyzed was the DR data obtained at the 24 h mark, determined through GC-MS analysis and application of the fluorine balance. Table 2 provides the experimental matrix required to conduct these experiments. A second-order polynomial function was postulated to obtain an accurate model response:

$$DR_t, \% = \beta_0 + \beta_1 X_1 + \beta_2 X_2 + \beta_{11} X_1^2 + \beta_{22} X_2^2 + \beta_{12} X_1 \cdot X_2 \quad (6)$$

where X_i represent the experimental factors in the coded variables (X_1 temperature and X_2 humidity), β are the coefficients for each factor (and their interactions), and β_0 is the intercept.

In addition, response surface methodology was used to analyze the combined effect of the factors studied, and their relevance to select the most significant ones was determined.

2.2.3. HFO4E Detection Using NIR. Continuous absorbance measurements were made by using NIR equipment throughout the experiment. All data were recorded by using the OceanView application. Subsequently, they were plotted and analyzed using the OMNIC and WiRE softwares.

3. RESULTS AND DISCUSSION

To achieve the main objective of this work, which is to study the effect of the operating conditions on the physicochemical behavior of HFO4E gas, different vector gases (N_2, CO_2 or dry air) were used under continuous arcs for 1 day. Regardless of the vector gas, a 20:80 v:v ratio was used, providing a good dielectric strength. The influence of temperature (25, 60, and 120 °C) and humidity (0, 200, and 500 ppm) was evaluated.

First, the degradation products identified by the validated GC/MS methodology are shown in Table 3. They were obtained for three replicates performed for each vector gas at 60 °C and 200 ppm humidity (see experiments marked with r1, r2, and r3 in Table 2). Similar results were obtained for all three replicates according to the relative standard deviation (RSD) analysis.

Figure 4 shows an example of a chromatogram for a gaseous sample composed of 20% HFO4E and 80% air.

Figure 5 shows the quantification of the degradation products in percentages for the three replicate experiments. The standard deviation of the replicates performed for each degradation compound is plotted. Moreover, the RSD percentage for all of the degradation products observed is less than 20%. This value is considered acceptable considering the exceedingly small percentages of each of the products, ranging from 0.001% to 0.06%.

Table 3. Identified Compounds for Each Gas Mixture by GC-MS[a]

Observed degradation compounds	CO_2	N_2	Air
CF_4	x		x
CO_2	x	x	x
C_2F_6	x		x
CH_2F_2	x		x
C_2F_4	x	x	x
C_3HF_3			x
HF	x	x	x

[a]The mixture consists of 20% HFO4E and 80% vector gas at 60°C and 200 ppm distilled water.

3.1. Experimental Design. Once the reproducibility of the experiments was confirmed, an experimental analysis was performed using the Minitab program. A DOE analysis was performed to obtain a response surface, using the DR data obtained over 24 h of experiments. Table 4 presents the resulting data where X_1 stands for temperature and X_2 for humidity.

The total degree of freedom (TDF) is defined as the number of factors studied and their products. Analyzing the two statistical parameters (F-value and p-value) for air shows that the order of significance of the terms is X_2^2 and X_1^2. Therefore, the model is minimally affected by the temperature and the temperature−humidity interaction.

Conversely, for CO_2, the only significant term is X_1 (temperature). The rest of the terms are clearly insignificant due to both the p-value, which exceeds 0.05 in all cases, and the F-value, which is relatively low.

Finally, looking at the p-values for N_2, the most significant terms are X_2, X_1^2, and X_2^2. Notably, the term X_1X_2 presents the best p-value but is considered insignificant because the F-value is too large.

The Figure S1 (see Supporting Information) shows the distribution of the model-predicted data versus the actual experimental values for each vector gas (air, CO_2, and N_2).

Figure S1a, corresponding to air, demonstrates a good approximation between the experimental and modeled values, fitting the bisector. Thus, the value of the coefficient of determination (R^2) gives an acceptable value (0.915). However, the plot of the externally studentized residuals (Figure S1b air) indicates a less satisfactory fit. Despite the close proximity to the regression line, more data points deviate noticeably from the regression line, suggesting that, in the case of air, the data do not fit the model obtained.

The diagnostic plots in Figure S1a, corresponding to the vector gas CO_2, show a distribution of the predicted and actual values along the straight line, indicating an excellent fit for both data. In addition, the value of the coefficient of determination is better than that for air (R^2 = 0.950). Similarly, the normal percentage probability and externally studentized residual plots (Figure S1b of CO_2) fit the regression line very well. This further confirms the excellent fit and accuracy of the model for the CO_2 vector gas.

Finally, for N_2, the diagnostic plots in Figure 6a indicate that the data for the predicted and actual values are quite close, even though they do not completely fit the bisector. Nevertheless, the

https://doi.org/10.1021/acs.iecr.3c03835
Ind. Eng. Chem. Res. 2024, 63, 2916−2931

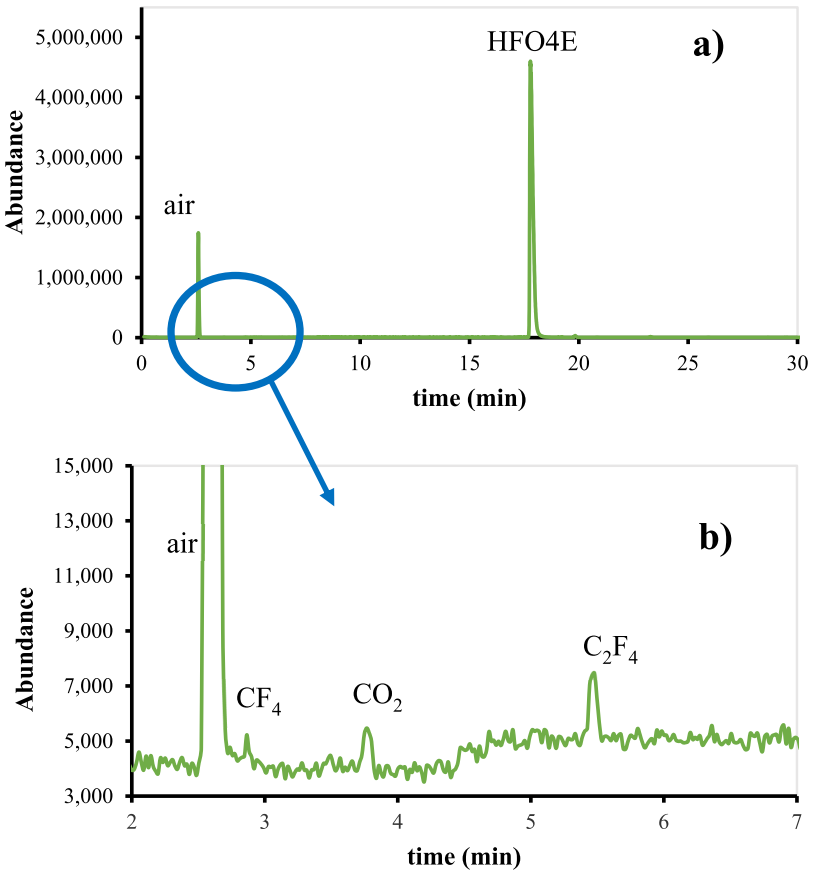

Figure 4. Chromatogram overview for a gaseous sample composed of 20% HFO4E and 80% air at 200 ppm and 60 °C (a) the same chromatogram between 2 and 7 min.

coefficient of determination (R^2) is the second best of the three vector gases with a value of 0.919. In addition, it is worth noting that the externally studentized residual plots (Figure S1b, for N_2) exhibit an excellent fit, being the ones that best follow the regression line among all of the vector gases. This shows a better fit to the model, although it is not as good as the performance achieved with CO_2.

The fit of the predicted data to the experimental data was analyzed, and the significance of each parameter and their interactions were evaluated to obtain the predicted DR. Initially, when examining the interaction between temperature (X_1) and humidity (X_2) for air, it becomes evident that this interaction is not statistically significant, as the p-value is 0.449 (see Table 4). However, the quadratic terms are noticeably significant, particularly in the case of temperature (with a p-value of 0.001). Consequently, an increase in the temperature factor results in a considerable increase in the degradation rate for air. The empirical model in terms of coded factors for the predicted degradation rate is given in eq 7.

$$DR_t,\ \%(\text{air}) = 0.1580 - 2.77\cdot10^{-3}X_1 - 1.51\cdot10^{-4}X_2 + 1.87\cdot10^{-6}X_1^2 + 2.8\cdot10^{-7}X_2^2 - 3.7\cdot10^{-7}X_1\cdot X_2 \quad (7)$$

The interaction between parameters X_1 and X_2 (temperature and humidity, respectively) is not significant in the case of CO_2, and the p-value obtained is greater than 0.05. Similarly, the only parameter that shows great significance is the temperature with a p-value of 0.034. The humidity factor is clearly of little significance since the p-value for its influence alone or with its own interaction is close to 1, demonstrating its lack of influence on the degradation rate.

The empirical model in terms of coded factors for the predicted degradation rate is listed in eq 8.

$$DR_t,\ \%(CO_2) = 0.0526 + 4.48\cdot10^{-4}X_1 + 3.36\cdot10^{-5}X_2 - 4.55\cdot10^{-4}X_1^2 - 2.1\cdot10^{-6}X_2^2 - 3.3\cdot10^{-5}X_1\cdot X_2 \quad (8)$$

Analyzing the interaction between the operating parameters for N_2 showed that the interaction between temperature (X_1) and humidity (X_2) is highly significant with a p-value of <0.001, indicating that an increase in both factors will cause a significant increase in the degradation rate. Similarly, the rest of the factors are also significant, except for temperature alone, whose p-value is close to unity.

The empirical model in terms of the coded factors for the predicted degradation rate is given in eq 9.

$$DR_t,\ \%(N_2) = 0,\ 07679 - 3.7\cdot10^{-5}X_1 - 2.09\cdot10^{-4}X_2 - 4.07\cdot10^{-6}X_1^2 + 1.3\cdot10^{-7}X_2^2 + 2.49\cdot10^{-6}X_1\cdot X_2 \quad (9)$$

Once the expressions for obtaining the theoretical DR for each vector gas were obtained, the designed model was validated. For this purpose, three experiments were carried out with random values of the factors analyzed (temperature and humidity), and the standard deviation percentage was calculated for each vector gas. It was observed that the predicted results were remarkably similar to the experimental results with no

https://doi.org/10.1021/acs.iecr.3c03835
Ind. Eng. Chem. Res. 2024, 63, 2916−2931

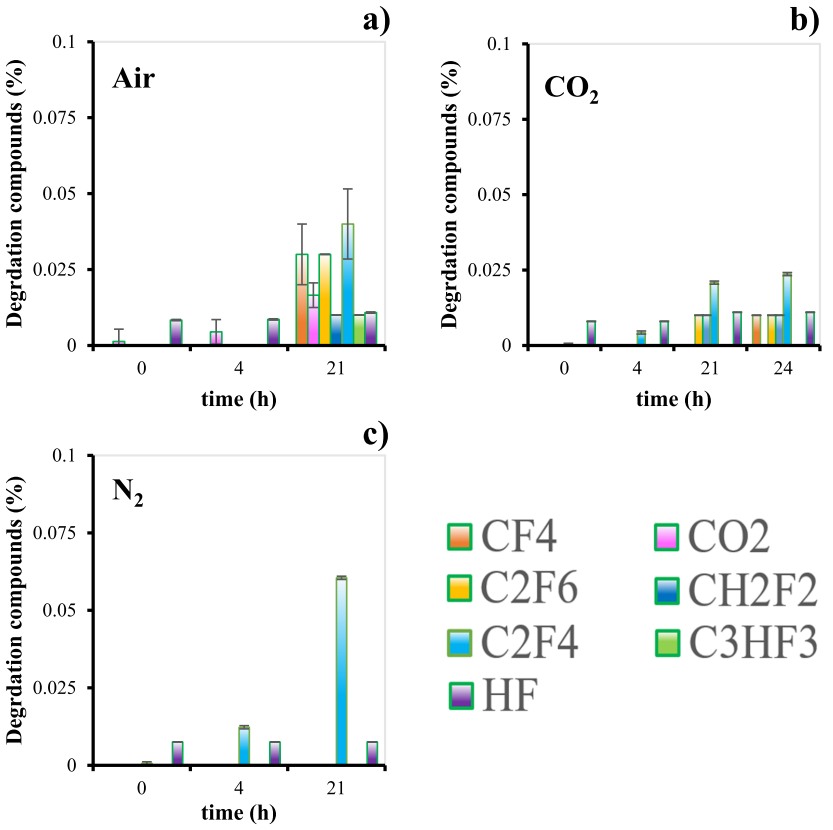

Figure 5. Variation of the concentration of degradation products observed in three experiments chosen for (a) air, (b) CO_2, and (c) N_2.

Table 4. Statistical Values Obtained by a DOE Study for Mixtures of HFO4E with Each Vector Gas

		Air		CO_2		N_2	
Source	TDF	F-value	p-value	F-value	p-value	F-value	p-value
Model	5	12.35	**0.002**	2.11	0.179	28.55	**<0.001**
X_1	1	2.22	0.179	6.87	**0.034**	0.01	0.909
X_2	1	3.99	0.086	0.00	0.990	17.77	**0.004**
X_1^2	1	34.02	**0.001**	1.45	0.267	6.53	0.038
X_{21}^2	1	6.33	**0.040**	0.02	0.887	5.71	**0.048**
X_1X_2	1	0.64	0.449	0.37	0.562	120.90	**<0.001**
Lack of fit	3	210.63	<0.001	55.35	0.001	1.47	0.350

significant difference between them. This excellent prediction is further confirmed by the value of the RSD (Table S1 of Supporting Information), which is ≤10% in all cases, highlighting its excellent reproducibility.[34] In addition, as previously shown by the coefficients of determination, the predicted DR for the CO_2 vector gas presented the best fit.

3.1.1. Significant Variables of Degradation. The arc effect (intensity 0.37 kJ/L·day) was first analyzed using air as a vector gas. Figure 6a−c show a general minimization of the degradation rate of HFO4E for the intermediate temperatures. Regarding humidity, and to a somewhat lesser extent temperature, a distinct impact on degradation becomes apparent, particularly at high humidity levels, resulting in a minimum degradation condition. Moreover, a reduction in degradation is noticeable starting from the fourth hour, particularly under extreme conditions of both high temperature (120 °C) and high humidity (500 ppm).

Figure 6d illustrates the response surface for air, reaffirming the observations made in the other graphs (Figure 6a−c). It clearly demonstrates the minimization of HFO4E degradation at intermediate temperatures and humidities. Conversely, the most significant degradation is evident at low temperatures (25 °C) across the entire humidity range, with the most pronounced effects observed under extreme conditions (0 and 500 ppm).

The same analysis was conducted for CO_2 (Figure S2), showing a minimization of the degradation effect of HFO4E at intermediate humidities at maximum temperature (120 °C). The results demonstrate that the higher the humidity, the greater the degradation. To conclude, we should also mention the condition of minimum degradation observed at high humidities and medium temperatures. Analyzing the degradation rate on the response surface, the opposite scenario becomes evident for intermediate values of both temperature and humidity, resulting in greater degradation. Furthermore, in the case of CO_2, the lowest degradation occurs at elevated temperatures over the entire humidity range (especially at 500 ppm).

Finally, for the N_2 vector gas (Figure S3), a lower degradation occurs with increasing temperature, except at high humidity, where the reverse condition occurs.

https://doi.org/10.1021/acs.iecr.3c03835
Ind. Eng. Chem. Res. 2024, 63, 2916−2931

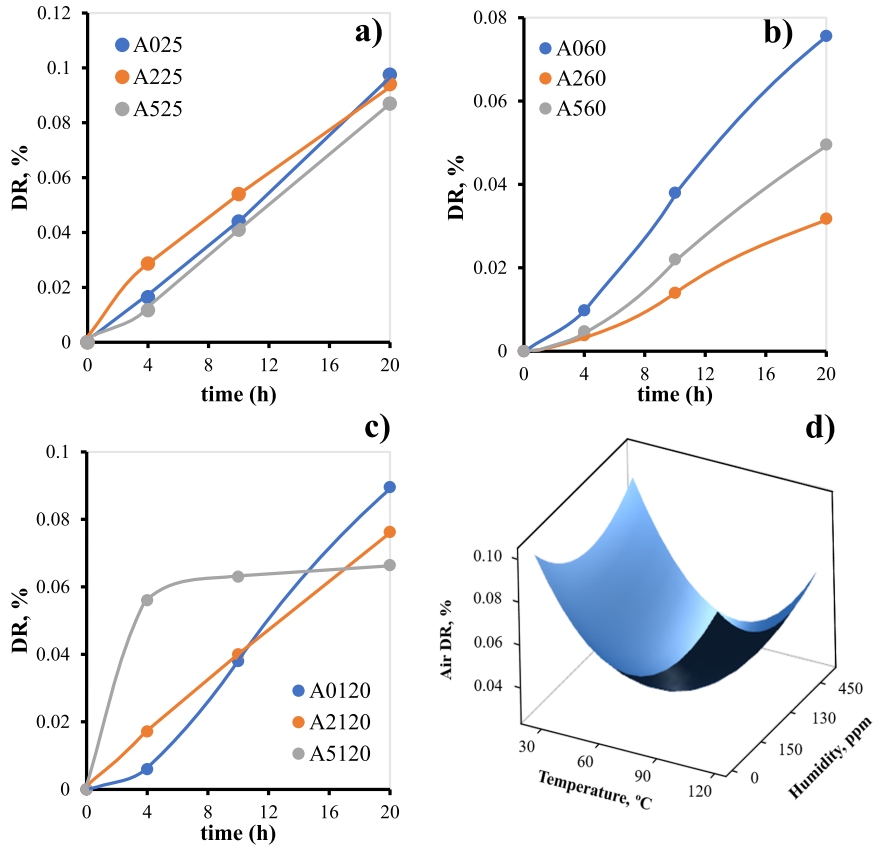

Figure 6. Evolution of the DR of HFO4E with gas vector air over time for each humidity condition at constant temperature (a−c) and response surface obtained using the Minitab tool (d).

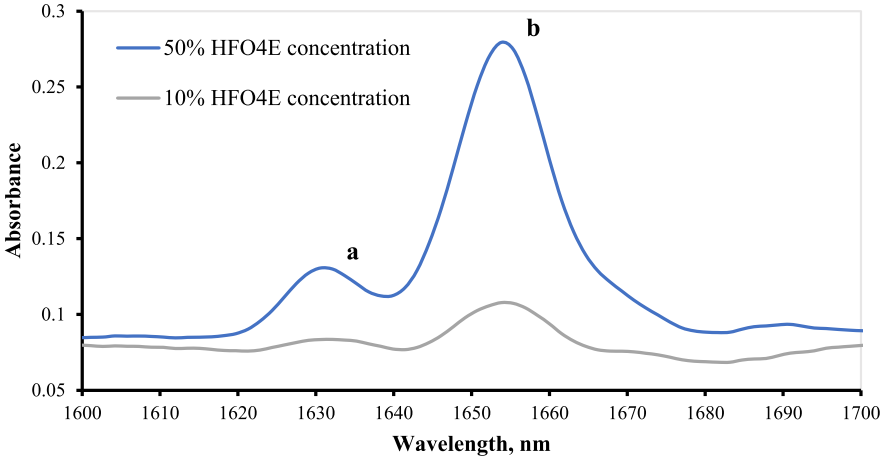

Figure 7. Spectra obtained for a mixture of 50% and 10% of HFO4E with air, plotted with the WiRE program.

Analyzing the response surface for this gas reveals two distinct minima and two maxima in the degradation of HFO4E, which are opposite, in terms of their operating conditions. The minima are reached at two very specific conditions, one being obtained at 25 °C and high humidity and the other at 120 °C and low humidity.

3.2. HFO4E Detection by NIR. In Figure 10, NIR spectra obtained over a range of 1600−1700 nm are shown. Two absorption bands appeared at 1630 and 1654 nm, corresponding to the concentration of HFO4E.

Apart from experimental measurements, a simulation was carried out by using the Gaussian code, confirming the experimental spectra. The simulation accounted for anharmonicity to capture the appearance of overtones and combinations. This was necessary because the wavelengths in question fall within the overtone region, specifically at 700 and 1600 nm.[35,36] Analyzing the anharmonic modes revealed two overtones (Figure 7a) at 1645 nm (very weak) and 1660 nm, exhibiting a slight shift to the right compared to the spectrum obtained experimentally. These overtones correspond to two C−H vibrations (Figure 7b), which appear at approximately 3125 nm. The combination of these two vibrations is located at 1661 nm, which is characteristic of C−H vibrations (Figure 8).

https://doi.org/10.1021/acs.iecr.3c03835
Ind. Eng. Chem. Res. 2024, 63, 2916−2931

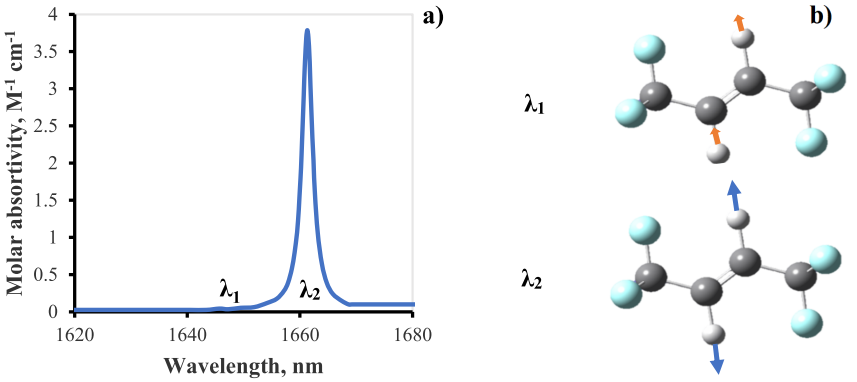

Figure 8. Theoretical spectrum obtained by Gaussian simulation (a) and its corresponding C−H vibrations (b).

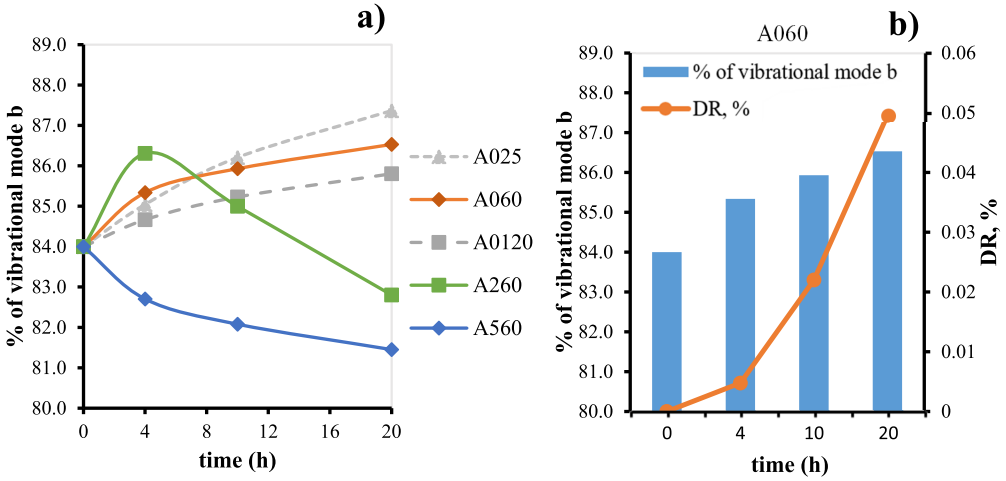

Figure 9. Evolution of vibrational mode *b* with time for a mixture of HFO4E with air vector gas at different operating conditions (a) and evolution of vibrational mode *b* and DR with time for the air vector gas at operating conditions of 0 ppm and 60 °C (b).

Therefore, the changes in the absorption band corresponding to 1654 nm were attributed to the degradation of HFO4E over time, owing to the high intensity associated with C−H vibrations in this region.

Two absorption bands were detected and confirmed to correspond to two conjugated vibrational modes. One of these two states corresponds to a (weak) vibrational mode *a*, which is located at a wavelength of 1630 nm (λ_1). The other vibrational mode, *b* (strong), appears at a wavelength of 1654 nm (λ_2).

Moreover, it was determined that these two absorption bands show an exchange. This is confirmed by the observation that as the absorbance of *a* increases, the absorbance of *b* decreases, and vice versa. The absorbance of the two bands obtained in each test was therefore quantified.

Prior to the study of each specific case, a calibration curve was built at HFO4E concentrations of 50%, 40%, 20%, 10%, and 5% (using air as a vector gas to reach 100%). To study the evolution of the different terms involved in these vibrational modes and absorbances, Beer−Lambert's Law[37] was applied.

The objective of employing these relationships is to derive the concentrations of each vibrational mode through the calculation of their respective molar absorptivity and by measuring the absorbance of each absorption band. In our specific case study, as shown in Figure 7, the absorption bands for vibrational modes *a* and *b* are remarkably close at 1630 and 1654 nm, respectively.

The previous calibration demonstrated a linear relationship between the absorbance and HFO4E concentration. Furthermore, these data show an excellent fit, as evidenced by the correlation coefficient values obtained for the evolution of each term, as shown in Figure S4 (Supporting Information).

Figure S4 illustrates that the molar absorptivity of vibrational mode "*a*" at wavelength λ_2 is 1 order of magnitude lower than at wavelength λ_1. This observation aligns with the observation that the vibrational mode *a* primarily appears at λ_1 (1630 nm). A similar pattern is noticeable for vibrational mode *b*, suggesting its lower absorptivity with respect to wavelength λ_1.

Once the values of the molar absorptivities were obtained, we proceeded to study the evolution of the two vibrational modes, depending on the vector gas and the operating conditions (humidity and temperature). As previously mentioned, we considered the vibrational modes as a predegradation step, as they are associated with strong C−H vibrations that can lead to a rupture of these C−H bonds.

Therefore, to analyze the effect of these modes on degradation, a study based on the evolution of the percentage of the vibrational mode *b* was conducted. This is because *b* is the strongest vibrational mode and, therefore, the most prone to degradation. Moreover, it has been experimentally demonstrated that both modes undergo changes with time. To obtain each mode's percentage, the concentration obtained from the band *b* was divided by the total (which would refer to the sum of the two absorption bands). The aim of this calculation was to compare in a more visual way the variation of the contribution of each vibrational mode with time.

https://doi.org/10.1021/acs.iecr.3c03835
Ind. Eng. Chem. Res. 2024, 63, 2916−2931

Table 5. Theoretical Reactions Proposed for the Decomposition of HFO4E

Reaction number	Reaction pathway	Barrier height (kcal mol^{-1})
	No participation of moisture H/OH	
R_{01}	$CF_3CH{=}CHCF_3 \rightarrow CF_3CH{=}C{=}CF_2 + HF$	75.20 (TS1)
R_{02}	$CF_3CH{=}CHCF_3 \rightarrow CF_3C{=}CHCF_2 + HF$	78.28 (TS2)
R_{a3}	$CF_3CH{=}CHCF_3 \rightarrow CF_3CH{=}CH + CF_3$	99.68
R_{a4}	$CF_3CH{=}CHCF_3 \rightarrow CF_3CH{=}CHCF_2 + F$	101.31
R_{a5}	$CF_3CH{=}CHCF_3 \rightarrow CF_3C{=}CHCF_3 + H$	110.92
R_{a6}	$CF_3CH{=}CHCF_3 \rightarrow CF_3CH + CF_3CH$	190.20
	Participation of moisture H/OH	
R_{m1}	$CF_3CH{=}CHCF_3 + H \rightarrow CF_3C{=}CHCF_3 + H_2$	23.82 (TS3)
R_{m2}	$CF_3CH{=}CHCF_3 + H \rightarrow CF_2CH{=}CHCF_3 + HF$	13.46 (TS4)
R_{m3}	$CF_3CH{=}CHCF_3 + OH \rightarrow CF_2CH{=}CH_2CF_3 + FOH$	61.74 (TS5)
R_{b4}	$CF_3CH{=}CHCF_3 + OH \rightarrow CF_3C{=}CHCF_3 + H_2O$	5.01 (TS6)
R_{b5}	$CF_3 + H \rightarrow CF_3H$	−102.43
R_{b6}	$CF_3 + OH \rightarrow CF_3OH$	−104.12
R_{b7}	$F + H \rightarrow HF$	−131.96
R_{b7}	$F + OH \rightarrow FOH$	−42.09

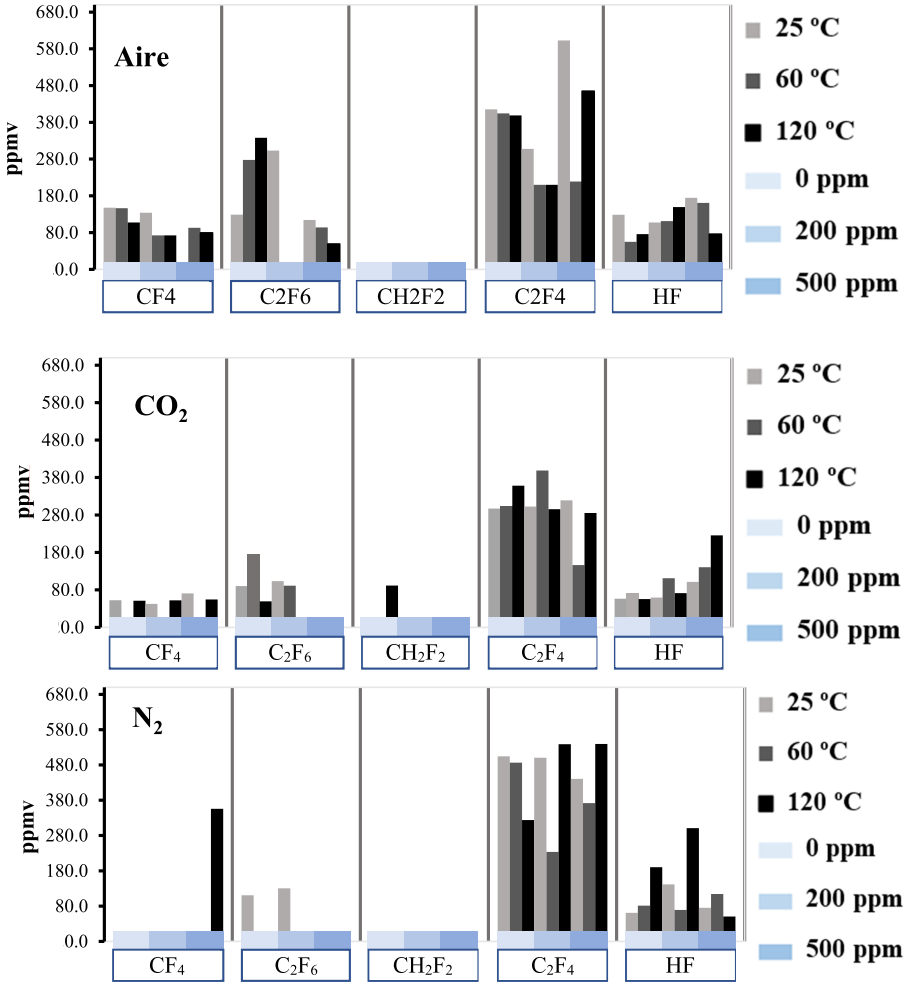

Figure 10. Degradation gases for each vector gas; temperature and humidity effect.

First, Figure 9a shows the evolution of the vibrational mode *b* with time for the air vector gas under different operating conditions. Remarkably, in this series of data, the factor that determines the tendency of the evolution of vibrational mode *b* is the humidity, causing a maximum condition (Figure 9a, A260) after 4 h under intermediate humidity (200 ppm). Conversely, the decline in the percentage of the vibrational mode *b* suggests its involvement in the degradation process, with a more significant contribution detected at higher humidities (500 ppm). Hence, considering the rise observed at lower humidities

https://doi.org/10.1021/acs.iecr.3c03835
Ind. Eng. Chem. Res. 2024, 63, 2916−2931

(A025, A060, and A0120), the factor promoting degradation is the less robust vibrational mode, namely, mode *a*. In conclusion, for the use of air, moisture has the most substantial impact on the evolution of the vibrational modes and, consequently, on the degradation process.

Figure S5 shows the evolution of the vibrational mode *b* for different temperatures and humidities for vector gas N_2. Figure S5a shows a clear similarity for air under intermediate conditions (200 ppm and 60 °C), with the same maximum effect. In contrast, at medium temperature conditions (60 °C) and extreme humidity values, the species responsible for the degradation is opposite to that of air, i.e., at 0 ppm, degradation is initiated by mode *b*, and at 500 ppm by mode *a*.

Analyzing Figure S5 and considering the exchange ratio of the two modes confirm that at intermediate humidities the degradation is first determined by mode *a* up to 4 h and then promoted by mode *b*.

The behavior of the CO_2 vector gas is similar to that of air, excluding the intermediate conditions (60 °C and 200 ppm), where the optimum condition at 4 h is not observed. Figure S6b reveals a clear decrease in vibrational mode *b* accompanied by an increase in DR, indicating its participation in the degradation at extreme humidity conditions (500 ppm) and intermediate temperatures (60 °C).

Based on these results, it can be concluded that mixtures with CO_2 and air coincide in terms of the dominant vibrational mode for all temperature and humidity conditions. However, mixtures with N_2 show identical mode evolution only at intermediate conditions (200 ppm and 60 °C), where the degradation is initially initiated by mode *a*, whereas mode *b* becomes dominant after 4 h. Consequently, for the mixture containing N_2 (contrary to air and CO_2), the degradation is initiated by mode *b* at a low humidity (0 ppm) and by mode *a* at a high humidity (500 ppm).

3.3. Stability at Short Time Periods. In the interpretation of HFO4E degradation, we also considered the emergence of degradation compounds resulting from the current production tests described earlier. Despite the average rate of energy loss during these tests being approximately 0.37 kJ/L·day, it is essential to note that the localized stress in each discharge is exceedingly high, leading to temperatures on the order of 6,000 K.[33] Under these extreme conditions, clearly endothermic reactions, which play a significant role in density functional theory (DFT) and transition states (TS), are favored and responsible for many of the substantial reactions observed. A compilation of the reactions considered[17] for the decomposition of HFO4E is given in Table 5. Here, the first six reactions appear to be the most relevant for the onset of degradation, and increasing endothermic character of the potential barrier can be observed. According to these estimations, the most probable processes are R_{01} and R_{02}, corresponding to state transitions. These processes are generated by vibrational modes *a* and *b* in accordance with the results of the previous section. The great significance of R_{01} and R_{02} in the onset is also confirmed by the presence of HF regardless of the vector gas, as shown in Figure 10.

Following the order presented in Table 5, we determined the R_{a4} and R_{a5} processes, potentially leading to the formation of HF.[17] However, these reactions require a higher energy input and, consequently, have lower probabilities of occurrence compared to those of R_{01} and R_{02}. Consequently, reaction R_{03}, with a relatively low potential barrier, assumes significance following the preceding processes due to the generation of a CF_3 radical. This radical is highly reactive and readily combines to produce C_2F_6, which, in accordance with the results obtained, emerges as the third most important degradation product after C_2F_4 and HF.

The fragmentation of the 4 and 3 carbon radicals originating from reactions R_{02} and R_{03} typically involve the stepwise removal of CF_2 and CF_3 groups, ultimately resulting in the production of C_2H_2. While this might raise concerns due to the high flammability of C_2H_2 at volumetric concentrations between 2.3% and 72.3%, it is important to note that this study indicates the absence and no concentration of C_2H_2, making this scenario highly unlikely. Consequently, an evolution toward the formation of 2-carbon gases by the cleavage of 4-carbon radicals seems more likely, although, as mentioned above, 2-carbon gases may also be obtained from the combination of two CF_3 radicals. As suggested by other authors,[38] this could be the most important mechanism to form higher structures by recombination of radicals. Even though 2- and 3-carbon radicals are highly reactive, according to density functional theory (DFT), the only relevant reactions are those involving radicals generated from the breakdown of water. However, these reactions are very unlikely to occur, as examining the presence of moisture reveals.

C_2F_4, the most abundant decomposition gas, is obtained through degradation by cleavage of the double bond. However, it does not seem to be the most plausible option because of the high energy barrier of 190.2 kcal/mol (reaction R_{a6}, Table 5). The results suggest that the radical generated in reaction R_{02}, along with reactions R_{a4} and R_{a5}, serves as the primary precursor for fragmentation, leading to the production of 2-carbon gases. For example, the $CF_3{-}C{=}CH{-}CF_2$ radical transforms into the $CF_2{=}CF{-}CH{=}CF_2$ radical by shifting the central double bond, which is likely facilitated by the relatively low potential barrier (31.28 kcal/mol). Subsequently, the cleavage of the central bond in $CF_2{=}CF{-}CH{=}CF_2$ results in the formation of $CF_2{=}CF$ and $CH{=}CF_2$ radicals, requiring an additional net energy of only 36.22 kcal/mol.

While direct cracking of the $CF_3C{=}CH{-}CF2$ radical into these two-carbon compounds is possible, it is unlikely due to the higher energy requirement of 98.7 kcal/mol. This hypothesis is further supported by the higher concentration of fluorine in the two-carbon gases, explaining the elevated concentration of C_2F_4.

Following the analysis of the degradation of HFO4E, the degraded gases were identified and quantified. Additionally, the effect of various operating conditions (carrier gas, temperature, and humidity) on the appearance of each of the degraded gases was investigated.

Examining the data on the degradation compounds reveals that they align with the data obtained with regard to their formation. When evaluating potential variations in light of the conducted experiments, it is important to note that CH_2F_2 is notably absent. Thus, humidity and the resulting production of H_2 do not seem to be responsible for this absence. This is further confirmed by the low concentration of H_2, with the exception of experiments involving CO_2.

The dominant degradation gas is C_2F_4. It does not show a clear trend in terms of its behavior with exposure to humidity. This supports the theory that the molecule results from the degradation of 4-carbon structures, as explained above. The influence of humidity does not appear to be supported, as no hydrogen-containing compounds are observed among the degradation products, except for HF, resulting from the most fundamental reactions (R_{01} and R_{02}). HF shows a higher formation intensity at high humidities, particularly in the case of CO_2. Hence, this is the only scenario in which a stronger

https://doi.org/10.1021/acs.iecr.3c03835
Ind. Eng. Chem. Res. 2024, 63, 2916−2931

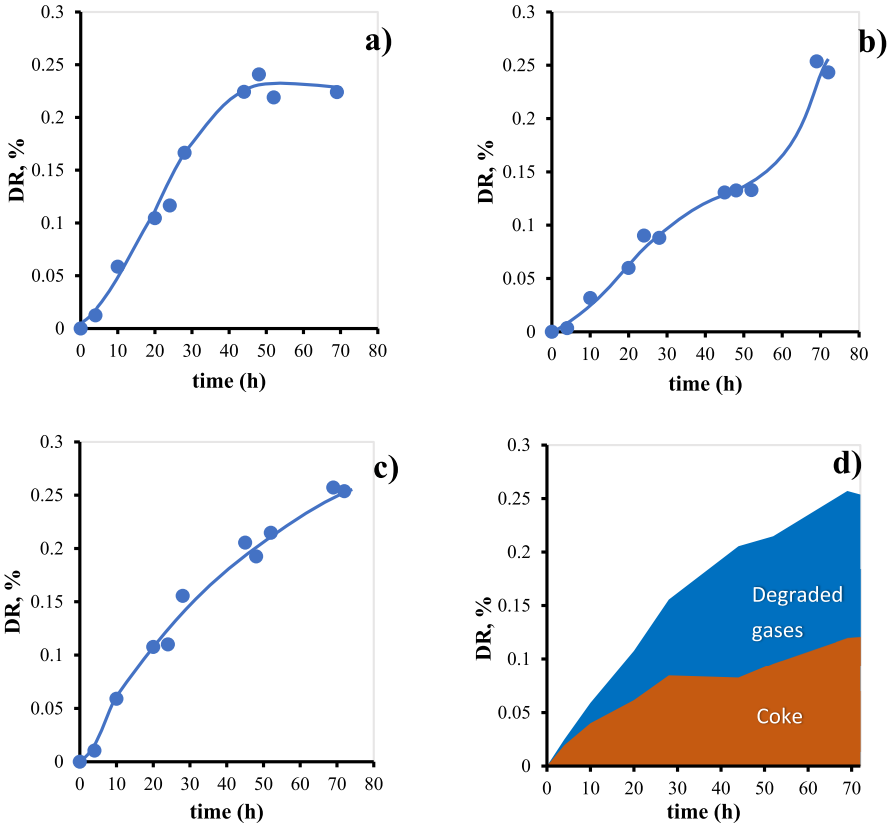

Figure 11. Evolution of the HFO4E degradation rate over an extended period of time for different vector gases: air, N_2, and CO_2 (a−c) and contribution to % DR of degraded gases and coke, with CO_2 as vector gas (d).

potential connection to humidity (in addition to the emergence of CH_2F_2) might be considered.

Regarding the other gases, it is reasonable to suggest that C_2F_6, C_2F_4, and CF_4 are of lesser significance, potentially formed through the combination of CF_3 with fluorine. These gases are mainly formed at low and medium humidities (0 and 200 ppm).

Regarding the vector gases, the case of N_2 shows a hugely different behavior from both air and CO_2, with a lower number of degradation compounds but a higher concentration of degraded compounds. This is primarily because the other species (C_2F_4, C_2F_6, and CH_2F_2) are present only in minute concentrations, likely due to their transformation into C_2F_4. It can therefore be concluded that in the presence of N_2, the degradation pathways are redirected toward the formation of C_2F_4.

CO_2 typically exhibits degradation components in smaller quantities. However, it may be necessary to quantify some of the coke formed in the same tests, a topic that will be explored in subsequent studies.

Regarding the effects of the degradation products observed in the tests, HF is commonly known to exhibit a notably high toxicity and corrosiveness, posing potential risks to both equipment and maintenance personnel.[39] However, no signs of corrosion were detected in the cell during the ongoing closing tests at the Ormazabal Energy Laboratory. In other words, if HF is present, it appears to be in such minute quantities that it does not impact the hermetic tank of the cell.

C_2F_6 exhibits a very high GWP of 9,200 CO_2eq over 100 years,[16] as well as a remarkable atmospheric lifetime of 10,000 years,[15] as discussed at the beginning of this paper (Table 1). CF_4 and C_2F_4 are considered two of the most harmful PFCs, due to their long lifetime. Moreover, CF_4 is the simplest PFC, with a GWP of 6,630 and an atmospheric lifetime of 50,000 years.[39] In addition, CF_4 is a species that is unlikely to cause significant reduction in dielectric strength.[40]

3.4. Stability at Extended Period of Times. To complement the degradation study of the HFO4E, a carbon balance was performed assuming that HFO4E degrades mainly toward the formation of fluorinated gases and solid carbon (coke). These studies were conducted for prolonged periods of discharges.

The evolution of the degradation rate over a long discharge period (72 h) exhibits two clear trends, as shown in Figure 11. Air (Figure 11a) shows a clear decrease of the degradation rate during the experiment and stabilizes the DR. Thus, air presents the lowest DR at the end of the test but with higher increasing velocity compared to the other vector gases.

In contrast, in the case of N_2 (Figure 11b), although a small decrease in the degradation rate is initially observed for intermediate times, it subsequently shows a rebound, indicating an evident continuity in degradation.

CO_2, as depicted in Figure 11c, presents an intermediate scenario between the other two vector gases. While the degradation rate decreases, it does not stabilize as rapidly as with air. Moreover, they continue to degrade HFO4E.

Furthermore, Figure 11d supports the hypothesis mentioned in the previous section, which suggests that hydrofluoroolefin degrades solely to form fluorinated gases and solid carbon (coke).

Table 6 summarizes the results of the carbon balance carried out for CO_2, demonstrating that approximately 1/3 of reaction R_{01} in Table 6 may be responsible for the formation of coke from

https://doi.org/10.1021/acs.iecr.3c03835
Ind. Eng. Chem. Res. 2024, 63, 2916−2931

Table 6. Degradation Rate Data for the Mixture of HFO4E with the CO_2 Vector Gas and the Respective Parts of the Degraded Gases and Coke

Experiments	DR,%	DR_{coke},%	$DR_{deg.gases}$,%
C025	0.058	0.021	0.037
C060	0.057	0.020	0.037
C0120	0.050	0.018	0.032
C225	0.062	0.021	0.041
C260	0.069	0.024	0.045
C2120	0.018	0.006	0.012
C525	0.075	0.029	0.046
C560	0.047	0.017	0.030
C5120	0.058	0.021	0.037

the $CF_3CH{=}C{=}CF_2$ radical. According to TS theory, this results in the formation of a four-carbon cyclic structure[17] facilitating the formation of coke by progressive H and F removal.

The presence of moisture is considered by taking into account the decomposition of water to generate H, O and OH radicals:

$$H_2O + h\nu \rightarrow H + OH + h\nu \rightarrow OH \quad (10)$$

$$OH + h\nu \rightarrow H + O \quad (11)$$

These reactions have relatively high potential barriers of 115 and 166 kcal/mol, respectively, thus requiring a highly endothermic environment such as arc discharges. However, it seems unlikely that moisture decomposition is significantly involved in the formation of degradation products. As shown in Table 6, the involvement of OH and O radicals facilitates degradation compounds with oxygen involvement, which has not been detected in any of the experiments in this study. In a highly endothermic environment, alternative degradation pathways for two and three carbon structures are more favorable. These pathways might explain the presence of HF, as discussed earlier, resulting from reactions R_{01} and R_{02}.

Table 7 shows a summary of the results of % DR obtained for each gas vector, also with the specific effect of the variables temperature and humidity. % DR values correspond to the case of minimum temperature and humidity (25 °C and 200 ppmv), after 72 h electric arc tests (making). % DR results obtained are very similar for the three gases studied, highlighting particularly a tendency toward stabilization in the formation of coke, in the mixtures with CO_2, as can be deduced from Figure 11. The joint effect of temperature and humidity can be obtained mathematically, from the expressions 7 to 9 shown in section 3.1, where the significance of each of the two variables and the reliability degree of predicted results are also indicated according to the statistical analysis carried out.

Table 7. Comparative Effect of Vector Gas: Air, CO_2, and N_2 on the Degradation (% DR) of Hydrofluoroolefine HFO-1336mzzE, as well as the Specific Effect of Temperature and Humidity

Vector Gas	% DR (as coke)	% DR (total)	Temperature (25−60−120 °C)[a]	Humidity (0−200−500 ppmv)[a]
Air	0.078	0.224	H-L-H	H-M-H
CO_2	0.121	0.254	H-M-L	M-H-H
N_2	0.076	0.243	H-M-L	H-M-M

[a]Effect on% DR: H (high) or M (medium) or L (low) for each level of temperature (25−60−120 °C) and humidity (0−200−500 ppmv).

Table 7 also shows the qualitative effect of the temperature and humidity separately. Thus, with CO_2 and N_2, the temperature has a decreasing effect on the % DR: H−M−L (high−medium−low); i.e., % DR decreases with increasing temperature (25−60−120 °C). Both cases can be deduced from Figures S2 and S3 (Supporting Information), while the air gives a minimum value of % DR at the medium temperature (60 °C) and is therefore preferable. This behavior, already commented on above, could be explained by the fact that the temperature levels tested do not correspond to the whole chamber but to a certain localized area where the temperature can rise, because of the high current intensity, at high energy demand. Convective currents generated by local heating seem to influence a decrease in the % DR. In the case of air, the temperature presents a minimum: H−L−H, with a low % DR value corresponding to the temperature of 60 °C and therefore more recommendable.

The effect of humidity on % DR is generally increasing, the higher the humidity level, as in the case of CO_2: M−H−H (medium−high), for the humidities of 0−200−500 ppmv, respectively. In the case of air, humidity presents, as with temperature, a minimum: H−M−H; i.e. a medium value of % DR for a 200 ppmv humidity and therefore the most recommendable to use. This minimum and the one mentioned in the case of temperature, also for air, can be deduced from Figure 6.

4. CONCLUSIONS

The combination of HFO4E and a vector gas (N_2, CO_2, or dry air) in an 80:20 (v/v) ratio has been demonstrated to be highly stable under the studied conditions of electric arc, temperature, and humidity, with a % DR of approximately 0.1%. Consequently, it is anticipated that there will be no substantial alterations in the dielectric properties. The results suggest a performance comparable to that of SF_6.

The results exhibited excellent reproducibility following the replication of degradation tests (RSD < 13%). This can be attributed to the use of a custom-designed arc simulator specifically created for this study.

A model equation was derived for the three vector gases—CO_2, air, and N_2—using the Design of Experiments (DOE) approach to analyze the degradation rate (DR) of HFO4E. The order from best to worst fit among the vector gases was CO_2, followed by air, and then N_2.

The response surface analysis performed in the DR analysis revealed a large effect of humidity in conjunction with the influence of the vector gas. Intermediate and high local temperatures mitigate HFO4E degradation.

The examination of HFO4E degradation by Density Functional Theory (DFT) and Transition States (TS) theory revealed the existence of two vibrational modes, denoted as "a" and "b" (occurring at λ_a = 1630 nm and λ_b = 1654 nm in the Near-Infrared region). These vibrational modes are postulated as the source of the degradation compounds formed with the following concentration order: C_2F_4, HF, C_2F_6, CF_4, and CH_2F_2.

An analysis of HFO4E degradation after prolonged exposure to an electric arc was also conducted. The degradation rate exhibited a declining trend, tending toward stabilization over time for air and, to a lesser extent, for CO_2. Consequently, CO_2 is a preferable vector gas. Moreover, a tendency toward a constant value of approximately 0.12% in the DR, resulting in the formation of coke, should be highlighted.

https://doi.org/10.1021/acs.iecr.3c03835
Ind. Eng. Chem. Res. 2024, 63, 2916−2931

■ ASSOCIATED CONTENT

Supporting Information

The Supporting Information is available free of charge at https://pubs.acs.org/doi/10.1021/acs.iecr.3c03835.

This work presents an extensive experimental study in which different HFO4E mixtures are analyzed. Consequently, extensive complementary information to the data shown in the main manuscript has been obtained. It is divided into three important sections. Statistical data of the response surface analysis on the degradation rate (DR) of HFO4E. Detailed effect of humidity and temperature on DR with vector gases CO_2 and N_2. Vibrational modes of HFO-1336mzzE as precursors of degradation rate. (PDF)

■ AUTHOR INFORMATION

Corresponding Author

José Ignacio Lombraña − *Chemical Engineering Department, Faculty of Science and Technology, University of the Basque Country (UPV/EHU), 48940 Leioa, Spain;* orcid.org/0000-0001-5861-2390; Email: ji.lombrana@ehu.eus

Authors

Elisabeth Bilbao − *Chemical Engineering Department, Faculty of Science and Technology, University of the Basque Country (UPV/EHU), 48940 Leioa, Spain*

Xinyi Xia − *Chemical Engineering Department, Faculty of Science and Technology, University of the Basque Country (UPV/EHU), 48940 Leioa, Spain*

María Luz Alonso − *Analytical Chemistry Department, Faculty of Science and Technology, University of the Basque Country (UPV/EHU), 48940 Leioa, Spain;* orcid.org/0000-0002-2027-9411

Rosa María Alonso − *Analytical Chemistry Department, Faculty of Science and Technology, University of the Basque Country (UPV/EHU), 48940 Leioa, Spain;* orcid.org/0000-0001-9046-6602

Jesús Izcara − *Ormazabal Corporate Technology, Parque Empresarial Boroa, 48340 Amorebieta-Etxano, Spain*

Josu Izagirre − *Ormazabal Corporate Technology, Parque Empresarial Boroa, 48340 Amorebieta-Etxano, Spain*

Complete contact information is available at: https://pubs.acs.org/10.1021/acs.iecr.3c03835

Author Contributions

Conceptualization, J.I. (Jesús Izcara), J.I.L. (Jose Ignacio Lombraña) and J.I. (Josu Izaguirre); data curation, M.L.A. (Maria Luz Alonso) and E.B.(Elisabeth Bilbao); formal analysis, M.L.A.; funding acquisition, R.M.A. (Rosa Maria Alonso), J.I.L. and J.I. (Josu Izaguirre); investigation, M.L.A., E.B. and X.X. (Xinyi Xia); methodology, M.L.A., E.B., X.X. and J.I.: project administration, R.M.A. and J.I.L.; resources, R.M.A. and J.I.L.; supervision, R.M.A. and J.I.L.; validation, M.L.A.; writing—original draft, E.B. and X.X.; review and editing, R.M.A., M.L.A. and J.I. (Jesús Izcara). All authors have read and agreed to the published version of the manuscript.

Funding

The project RTC2019-006844-3 was supported by the Ministry of Science and Innovation (MCIN) and the State Agency for Innovation (AEI) of the Spanish Government. The authors would like to thank Aralar SL (Basauri, Spain) for their collaboration in the construction of the electric arc simulation equipment used specifically for this study.

Notes

The authors declare no competing financial interest.

■ REFERENCES

(1) Chmielak, W.; Daszczynski, T.; Pochanke, Z.; Wesolowski, M.; Szreder, R.; Obarski, N. Laboratory Tests of Medium Voltage Switchgear Isolators. *PAEE*. https://www.webofscience.com/wos/woscc/full-record/WOS:000411120200026.

(2) Fang, X.; Hu, X.; Janssens-Maenhout, G.; Wu, J.; Han, J.; Su, S.; Zhang, J.; Hu, J. Sulfur Hexafluoride (SF_6) Emission Estimates for China: An Inventory for 1990−2010 and a Projection to 2020. *Environ. Sci. Technol.* **2013**, *47* (8), 3848−3855.

(3) Tian, S.; Zhang, X.; Cressault, Y.; Hu, J.; Wang, B.; Xiao, S.; Li, Y.; Kabbaj, N. Research status of replacement gases for SF_6 in power industry. *AIP Adv.* **2020**, *10* (5), 050702.

(4) Zhang, X.; Lan, J.; Tian, S.; Rao, X.; Li, X.; Yuan, Z.; Jin, X.; Gao, S.; Zhang, X. Study of compatibility between eco-friendly insulating medium $C_6F_{12}O$ and sealing material EPDM. *J. Mol. Struct.* **2021**, *1244*, 130949.

(5) Widger, P.; Haddad, A.; Griffiths, H. Breakdown performance of vacuum circuit breakers using alternative CF3I-CO_2 insulation gas mixture. *IEEE Trans Dielectr. Electr. Insul.* **2016**, *23* (1), 14−21.

(6) Zhang, X.; Yu, L.; Gui, Y.; Hu, W. First-principles study of SF_6 decomposed gas adsorbed on Au-decorated graphene. *Appl. Surf. Sci.* **2016**, *367*, 259−269.

(7) Ritchie, H.; Roser, M.; Rosado, P. (2020). CO_2 and Greenhouse Gas Emissions. Our World in Data. https://ourworldindata.org/co2-and-other-greenhouse-gas-emissions.

(8) Wang, X.; Zhong, L.; Yan, J.; Yang, A.; Han, G.; Han, G.; Wu, Y.; Rong, M. Investigation of dielectric properties of cold C_3F_8 mixtures and hot C_3F_8 gas as Substitutes for SF_6. *Eur. Phys. J. D* **2015**, *69* (10). DOI: 10.1140/epjd/e2015-60327-9.

(9) Pachauri, R. K.; Meyer, L. Climate Change 2014: Synthesis Report. *Intergovernmental Panel on Climate Change*. 2015. https://archive.ipcc.ch/pdf/assessment-report/ar5/syr/SYR_AR5_FINAL_full_wcover.pdf.

(10) Devins, J. Replacement Gases for SF_6. *IEEE Trans Dielectr. Electr. Insul.* **1980**, *EI-15* (2), 81−86.

(11) Sovacool, B. K.; Griffiths, S.; Kim, J.; Bazilian, M. Climate change and industrial F-gases: A critical and systematic review of developments, sociotechnical systems and policy options for reducing synthetic greenhouse gas emissions. *Renew. Sust. Energy Rev.* **2021**, *141*, 110759.

(12) Li, Y.; Tian, S.; Zhong, L.; Chen, G.; Xiao, S.; Cressault, Y.; Fu, Y.; Zheng, Y.; Preve, C.; Cui, Z.; Zhang, Y.; Ye, F.; Piccoz, D.; Wang, G.; Li, Y.; Tu, Y.; Zhou, W.; Tang, J.; Zhang, X. Eco-friendly gas insulating medium for next-generation SF_6-free equipment. *IEEE Trans. Dielectr. Electr. Insul.* **2023**, *2* (1), 14−42.

(13) Restrictions under consideration. ECHA. https://echa.europa.eu/es/restrictions-under-consideration/-/substance-rev/72301/term.

(14) Gao, Z.; Luo, Y.; Peng, R.; Wang, X.; Yu, P.; Zhou, W. Investigation on insulation properties of HFO-1336mzz(E) and N_2/CO_2 mixtures as SF6 substitutes in gas-insulated electrical applications. *High. Volt.* **2023**, *8* (1), 48−58.

(15) Zhuo, R.; Chen, Q.; Wang, D.; Fu, M.; Tang, J.; Hu, J.; Jiang, Y. Compatibility between $C_6F_{12}O$-N_2 Gas Mixture and Metal Used in Medium-Voltage Switchgears. *Energies* **2019**, *12* (24), 4639.

(16) Xiao, S.; Zhang, X.; Tang, J.; Liu, S. A review on SF_6 substitute gases and research status of CF3I gases. *Energy Rep.* **2018**, *4*, 486−496.

(17) Liu, J.; Wang, F.; Zhong, L.; Gan, H.; Hai, B.; Tang, N.; Li, L.; Zhou, Y. Theoretical study of the decomposition mechanism of a novel eco-friendly insulation medium HFO-1336mzz(E) considering the effect of trace humidity. *J. Phys. D: Appl. Phys.* **2022**, *55* (4), 045201.

(18) Tanaka, K.; Ishikawa, J.; Kontomaris, K. K. Thermodynamic properties of HFO-1336mzz (E) (trans-1,1,1,4,4,4-hexafluoro-2-butene) at saturation conditions. *Int. J. Refrig.* **2017**, *82*, 283−287.

(19) Tang, N.; Xiong, J.; Zhou, Y.; Wang, K.; Zhang, B.; Li, X.; Sun, D. Insulation Performance of Environmental-Friendly Gas HFO-1336mzz (E) and Its Mixtures. *ECS Trans. Cn.* **2021**, *36* (13). DOI: 10.19595/j.cnki.1000-6753.tces.210164.
(20) Alonso, M. L.; Espinazo, A.; Alonso, R. M.; Lombraña, J. I.; Izcara, J.; Izaguirre, J. New Generation of SF_6-Free Medium-Voltage Switchgear for the Electrical Network: Stability and Toxicity Studies of Trans-1,1,1,4,4,4-Hexafluorobut-2-ene with N2 Gas Mixture. *Processes* **2023**, *11* (1), 136.
(21) Yoshida, T.; Koga, H.; Harada, T.; Miki, S.; Arioka, M.; Sato, S.; Yoshida, S.; Inoue, N.; Maruyama, A.; Takeuchi, T. Insulation technology in dry air and vacuum for a 72-kV low-pressure dry-air insulated switchgear. *Electr. Eng. Jpn.* **2011**, *175* (1), 18−24.
(22) Mizuno, T.; Morita, K.; Kurata, Y.; Miyagawa, H. The electrical performance of air or nitrogen gas with solid insulation and the application for switchgears. *IEEE PES T&D Conference and Exposition* **2002**, DOI: 10.1109/tdc.2002.1177728.
(23) Li, C.; Tang, J.; Zhao, Z.; Li, H.; Miao, Y.; Zeng, F. Decomposition Characteristics of SF_6/N_2 Under Partial Discharge of Different Degrees. *IEEE Access* **2020**, *8*, 192312−192319.
(24) Li, Y.; Qin, J.; Han, P.; Zhuo, R.; Wang, D.; Wang, Y.; Tang, J.; Zhang, X.; Xiao, S. Partial discharge induced decomposition properties and mechanism of HFO-butene/CO_2 as eco-friendly gas insulating medium. *IEEE Trans. Dielectr. Electr. Insul.* **2023**, 1.
(25) Xiao, S.; Han, P.; Li, Y.; Li, Z.; Ye, F.; Li, Y.; Tang, J.; Xia, Y.; Zhang, X. Insulation Performance and Electrical Field Sensitivity Properties of HFO-1336mzz(E)/CO2: A New Eco-friendly Gas Insulating Medium. *IEEE Trans. Dielectr. Electr. Insul.* **2021**, *28* (6), 1938−1948.
(26) Espinazo, A.; Lombraña, J. I.; Asua, E.; Pereda-Ayo, B.; Alonso, M. L.; Alonso, R. M.; Cayero, L.; Izcara, J.; Izagirre, J. Diffusional Behavior of New Insulating Gas Mixtures as Alternatives to the SF6-Use in Medium Voltage Switchgear. *Appl. Sci.* **2022**, *12* (3), 1436.
(27) Alonso, M. L.; Alonso, R. M.; Lombraña, J. I.; Izcara, J.; Izagirre, J. Exploring the Decomposition Products of 1,3,3,3-Tetrafluoropropene and Perfluoro-(3-methylbutan-2-one) Gas Mixtures in Medium-Voltage Electrical Switchgear as Alternatives to SF_6. *ACS Omega* **2021**, *6*, 21534−21542.
(28) Kujak, S.; Herried-Leehey, M.; Robaczewski, C. Chemical Stability Investigations of Ultra-Low GWP Refrigerants R-1336mzz-(Z), R-1336mzz(E), R-514A, R-1233zd(E), and R-1224yd(Z) with Lubricants. *Int. Refrig. Air-Cond. Conference* **2022**, 2384. https://docs.lib.purdue.edu/iracc/2384
(29) Huo, E.; Liu, C.; Xu, X.; Li, Q.; Dang, C.; Wang, S.; Zhang, C. The oxidation decomposition mechanisms of HFO-1336mzz(Z) as an environmentally friendly refrigerant in O_2/H_2O environment. *Energy* **2019**, *185*, 1154−1162.
(30) Huo, E.; Liu, C.; Xu, X.; Li, Q.; Dang, C. A ReaxFF-based molecular dynamics study of the oxidation decomposition mechanism of HFO-1336mzz(Z). *Int. J. Refrig.* **2018**, *93*, 249−258.
(31) Huo, E.; Liu, C.; Xu, X.; Li, Q.; Dang, C. A ReaxFF-based molecular dynamics study of the pyrolysis mechanism of HFO-1336mzz(Z). *Int. J. Refrig.* **2017**, *83*, 118−130.
(32) Wang, Y.; Ding, D.; Zhang, Y.; Yuan, Z.; Tian, S.; Zhang, X. Research on infrared spectrum characteristics and detection technology of environmental-friendly insulating medium $C_5F_{10}O$. *Vib. Spectrosc.* **2022**, *118*, 103336.
(33) Kawahara, N.; Hashimoto, S.; Tomita, E. Spark discharge ignition process in a spark-ignition engine using a time series of spectra measurements. *Proc. Combust Inst.* **2017**, *36* (3), 3451−3458.
(34) Aronhime, S. N.; Calcagno, C.; Jajamovich, G. H.; Dyvorne, H. A.; Robson, P. M.; Dieterich, D. T.; Fiel, M. I.; Martel-Laferrière, V.; Chatterji, M.; Rusinek, H.; Taouli, B. DCE-MRI of the liver: Effect of linear and nonlinear conversions on hepatic perfusion quantification and reproducibility. *J. Magn Reson Imaging* **2014**, *40* (1), 90−98.
(35) Beć, K. B.; Grabska, J.; Badzoka, J.; Huck, C. W. Spectra-structure correlations in NIR region of polymers from quantum chemical calculations. The cases of aromatic ring, C═O, C≡N and C−Cl functionalities. *Spectrochim Acta A Mol. Biomol Spectrosc.* **2021**, *262*, 120085.
(36) Analytical Vibrational Spectroscopy - NIR, IR, and Raman. 2020. *Spectroscopy Online*. https://www.spectroscopyonline.com/view/analytical-vibrational-spectroscopy-nir-ir-and-raman.
(37) Verhoeven, J. W. Glossary of terms used in photochemistry (IUPAC Recommendations 1996). *Pure Appl. Chem.* **1996**, *68* (12), 2223−2286.
(38) Li, Y.; Xiao, S.; Chen, Q.; Tang, J.; Chen, D.; Wang, D. Decomposition Properties of C_4F_7N/N_2 Gas Mixture: An Environmentally Friendly Gas to Replace SF_6. *J. Ind. Eng. Chem.* **2018**, *57* (14), 5173−5182.
(39) Anus, A.; Sheraz, M.; Jeong, S.; Kim, E. K.; Kim, S. Catalytic thermal decomposition of tetrafluoromethane (CF_4): A review. *J. Anal. Appl. Pyrolysis.* **2021**, *156*, 105126.
(40) Wang, W.; Murphy, A. B.; Rong, M.; Looe, H. M.; Spencer, J. W. Investigation on critical breakdown electric field of hot sulfur hexafluoride/carbon tetrafluoride mixtures for high voltage circuit breaker applications. *J. Appl. Phys.* **2013**, *114* (10), 103301.